System Design Considerations for the Retrieval of Sea Surface Temperatures in the NPOESS Era

KEITH D. HUTCHISON, STEVE MARUSA, JOHN R. HENDERSON, ROBERT C. KENLEY, PHILLIP C. TOPPING, WILLIAM G. UPLINGER, AND JOHN A. TWOMEY

Center for Remote Environmental Sensing Technology, Lockheed Martin Missiles & Space, Sunnyvale, California

(Manuscript received 6 August 1997, in final form 24 March 1998)

ABSTRACT

The National Polar-Orbiting Operational Environmental Satellite System (NPOESS) requires improved accuracy in the retrieval of sea surface skin temperature (SST_S) from its Visible Infrared Imager Radiometer Suite (VIIRS) sensor over the capability to retrieve bulk sea surface temperature (SST_B) that has been demonstrated with currently operational National Oceanic and Atmospheric Administration (NOAA) satellites carrying the Advanced Very High Resolution Radiometer (AVHRR) sensor. Statistics show an existing capability to retrieve SST_B with a 1σ accuracy of about 0.8 K in the daytime and 0.6 K with nighttime data. During the NPOESS era, a minimum 1σ SST_S measurement uncertainty of 0.5 K is required during daytime and nighttime conditions, while 0.1 K is desired. Simulations have been performed, using PACEOS™ scene generation software and the multichannel sea surface temperature (MCSST) algorithms developed by NOAA, to better understand the implications of this more stringent requirement on algorithm retrieval methodologies and system design concepts. The results suggest that minimum NPOESS SST_S accuracy requirements may be satisfied with sensor NEΔT values of approximately 0.12 K, which are similar to the AVHRR sensor design specifications. However, error analyses of retrieved SST_B from AVHRR imagery suggest that these more stringent NPOESS requirements may be difficult to meet with existing MCSST algorithms. Thus, a more robust algorithm, a new retrieval methodology, or more stringent system characteristics may be needed to satisfy SST_S measurement uncertainty requirements during the NPOESS era. It is concluded that system-level simulations must accurately model all relevant phenomenology and any new algorithm development should be referenced against in situ observations of ocean surface skin temperatures.

1. Introduction

With the earth's surface consisting of nearly 75% water, the ocean surface temperature plays an essential role in the global climate system. Most of the solar radiation reaching it is absorbed, stored, and redistributed by currents before escaping to the atmosphere largely as latent heat of evaporation and to a lesser extent as longwave radiation. The currents are driven by the exchange of momentum, heat, and water between the ocean and atmosphere (Houghton et al. 1990).

Global observations of sea surface temperatures (SSTs), wind stress over the oceans, and surface elevation of the ocean relative to the geoid are itemized by the World Climate Research Programme as being vital components of climate research that must be provided by satellite-borne instruments. Additionally, the minimum accuracy required of sea surface temperature measurements for climatological applications is specified as between $\pm 0.2-0.3$ K (Webster and Fieux 1984; Minnett 1986; Smith et al. 1996; Watts et al. 1996).

Operational satellite-derived sea surface temperatures analyses are based upon the regression of satellite-retrieved sea surface temperatures against bulk ocean temperatures measured by buoys (McClain et al. 1983; McClain et al. 1985; Walton 1988). These analyses (hereafter referred to as SST_B) provide a major source of information for ocean modeling and studies on oceanographic processes. Satellite observations provide over 95% of the real-time data needed to produce analyses of the thermal structure of the ocean, which are the bases for generating global and mesoscale dynamic ocean forecasts. Satellite-based SST_B observations are also used to evaluate forecast model skill and document changes in forecast accuracy resulting from model enhancements (Clancy and Sadler 1992).

The National Polar-Orbiting Operational Environmental Satellite System (NPOESS) requires improved accuracy in the retrieval of sea surface skin temperature (referred to hereafter as SST_S) over the capability to retrieve SST_B that has been demonstrated with operational National Oceanic and Atmospheric Administra-

Corresponding author address: Dr. Keith D. Hutchison, Lockheed Martin Missiles & Space, Advanced Technology Center, 3251 Hanover St., Org: H1-11 Bldg. 255, Palo Alto, CA 94304-1187.
E-mail: keith.hutchison@lmco.com

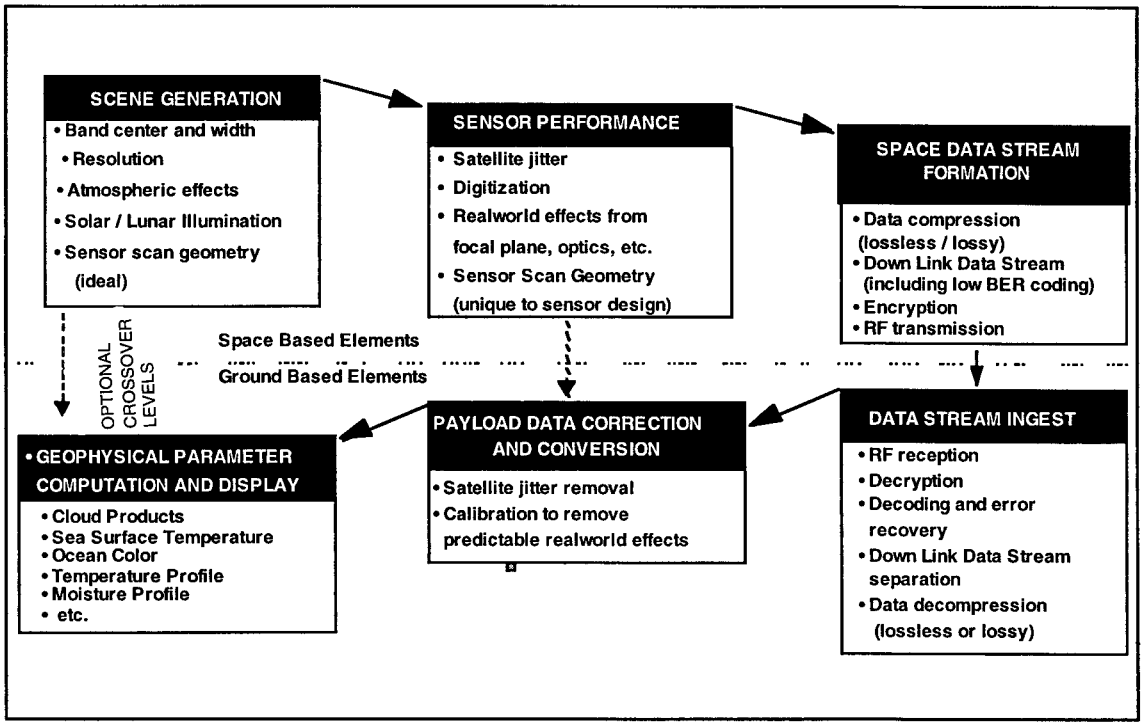

FIG. 1. Architecture of PACEOS™ software for scene simulation and retrieval of geophysical parameters.

tion (NOAA) satellites carrying the Advanced Very High Resolution Radiometer (AVHRR) sensor. Initial statistics based upon published results show a capability to retrieve global SST_B analyses with a 1σ accuracy of 0.78 K with daytime and 0.58 K with nighttime AVHRR imagery (Kenley 1994; McClain et al. 1983; McClain et al. 1985). A more recent comparison of different algorithms for deriving SST_B from AVHRR data indicates that there has been little improvement in this global analysis capability during the past decade (Barton 1995). In the NPOESS era, a 1σ SST_S measurement uncertainty of 0.5 K is required during daytime and nighttime conditions while 0.1 K is desired. This more stringent specification is applicable to both cloud-free and cloudy conditions as stated in the Sensor Requirements Document (SRD) for the Visible Infrared Imager Radiometer Suite (VIIRS) and the SRD for the Conical Scanning Microwave Imager Sounder (CMIS).

More specifically, the VIIRS SRD requires the retrieval of global SST_S with a 1σ measurement uncertainty of 0.5 K (which is subject to review for appropriateness and may be changed during the course of the program) during daytime and nighttime conditions for all cloud-free ocean surfaces and skin temperatures within the range of 271–313 K (VIIRS SRD 1997). For an ensemble of N estimates of SST_S, the measurement uncertainty ξ_N between the retrieved value of SST_S for the ith member of the ensemble SST_i and the members true value SST_T is given by

$$\xi_N = \left[\sum_{i=1,N} (SST_i - SST_T)^2/N\right]^{1/2}, \quad (1)$$

where the notation for SST_S has been changed to SST for simplicity. In addition, the maximum allowable SST_S measurement accuracy β_N is specified as 0.2 K and is defined as the magnitude of the difference between the mean estimated value of the SST_S and its true value; thus, for the same ensemble of N estimates, the measurement accuracy is written as

$$\beta_N = |\mu_N - SST_T|, \quad (2)$$

where

$$\mu_N = \left(\sum_{i=1,N} SST_i\right) \Big/ N. \quad (3)$$

2. PACEOS™ simulation software

End-to-end analyses of system design concepts on SST_S retrieval accuracy have been evaluated using a Lockheed Martin proprietary software package known as PACEOS™, an acronym for Performance and Analysis Capability for Earth Observation Systems (Marusa et al. 1997). An overview of the PACEOS™ architecture is shown in Fig. 1. PACEOS™ has been used successfully in the design process for a variety of satellite sensors including *Landsat-7*, DMSP Block 6, and the Lockheed Martin Commercial Remote Sensing System

(CRSS). PACEOS™ has also been used to evaluate the performance of several early warning airborne and space programs.

The PACEOS™ architecture consists of two major functional areas: 1) the generation of space-based elements shown in the top half of Fig. 1 and 2) a ground-based processing system seen in the lower half of the figure. The space-based elements functional area is divided into three major subsections: 1) the scene generation module, which calculates upwelling radiance arriving at the sensor aperture; 2) the sensor performance module where the energy (a) may be taken through a variety of optical parameters, (b) converted to electrical signals at the focal plane, and (c) processed prior to entering the 3) space data stream formation module, which packages the sensor data into the satellite data stream for transmission to the ground. Corresponding modules in the ground-based elements functional area contain advanced science algorithms to analyze data created in each module of the space-based elements. A short overview of each module in the space-based elements provides insight into the capabilities available for end-to-end simulations of sea surface temperatures or other retrieved products, commonly referred to as environmental data records (EDRs) in the NPOESS program.

a. Scene generation module

A primary use of simulation software is to predict the utility of future remote sensing systems using either a completely new design or a modification to an existing concept. To support these different applications, PACEOS™ was designed to be initiated from multiple data sources: imagery acquired from space-based (or airborne) sensors or a materials database that associates surface classification with emissivity and reflectivity characteristics. Next, sensor bandpasses are defined along with atmospheric conditions and external energy (solar or lunar) sources. Upwelling radiances are generated at satellite altitudes using a variety of atmospheric transmission codes that have been integrated into PACEOS™ using C and Motif interfaces. The current version includes interfaces to the full functionality of MODTRAN and RADTRAN (Berk 1989; Falcone et al. 1979). The resultant radiances, transmissions, and brightness temperatures are then extracted for use in the sensor performance module. Additionally, similar data can be input into PACEOS™ from measurements or calculations done offline by other software packages such as FASCODE (Clough et al. 1986). The output from the scene generation module of PACEOS™ is a two-dimensional file of radiances or brightness temperatures arriving at the sensor aperture.

The scene generation module provides the capability to specify a wide variety of conditions and vary each across the scene including: atmospheric profiles of all relevant meteorological conditions, cloud cover and cloud distributions, solar and/or lunar illumination, sensor scan or viewing angles, and surface material parameters such as temperature, emissivity, and topography. This flexibility has allowed PACEOS™ to fully support simulations of terrestrial scenes and it has also been used to model planetary scenes, such as the surface and atmosphere of Mars, for non-Earth viewing sensors.

The PACEOS™ architecture was also designed to be easily implemented on a variety of computer platforms. The spatial resolution is user defined, and scene dimensions can be as small as a 2×2 pixel array or much larger depending on the limitations of the computer platform(s) used in the simulation. PACEOS™ is most commonly used with a 1024×1024 pixel array with the DEC Alpha 600 platforms in the CREST Lab. Other features of PACEOS™ include the ability to subdivide large scenes into subsections and process each on a separate CPU, then merge results to further lower hardware requirements. Simulations can also be run interactively or from batch mode using files that completely define the simulation scenario.

It has frequently proven valuable to transfer the output of the scene generation module directly into the algorithms in the ground-based elements function of PACEOS™, thus bypassing the sensor and spacecraft effects. This process allows an early evaluation on the feasibility of meeting the EDR threshold requirements from a ''perfect'' or idealized sensor. In these cases, failure of an optimized retrieval algorithm to meet minimum or threshold EDR requirements, or meeting them with small margins, is a clear indication that a major system design modification or new algorithm retrieval approach may be necessary.

b. Sensor performance module

The sensor performance module supports sensor concept studies from two data sources: 1) a library containing the characteristics of numerous operational environmental satellite sensors and 2) sensor parameters created for a new design. The sensor performance module uses information on satellite altitude, scan angle, and instantaneous field of view to calculate pixel along-track and cross-track resolution. Modulation transfer functions (MTFs) are used to account for image degradation due to optical, motion, and atmospheric effects. The various MTFs may be input directly or calculated by PACEOS™ from design specifications. Additionally, optical and detector losses, radiation and electrical noise, and detector noise can be specified along with individual spectral response functions. Finally, it is also possible to include the effects of relative focal plane displacement due to phenomena such as thermal effects and jitter induced from either the spacecraft or the sensor. The output from this module is a file of digitized sensor data, up to 16-bits per pixel, which are subsequently calibrated and earth-located in the correspond-

ing payload data correction and conversion module of the ground processing system.

When the output of the sensor performance module is analyzed by advanced algorithms in the ground segment element, it is possible to quantitatively evaluate the accuracy of the retrieved EDR at each step of the system design process. This information is valuable for the early identification of system hardware drivers, which could provide valuable time to propose and evaluate alternatives to lower overall system costs.

c. Space data stream formation module

The space data stream formation module simulates the onboard processor functions necessary to prepare the sensor data for transmission to the ground processing system. Subsystem effects that can be simulated in the data stream formation module include such features as the fidelity of RF transmission and data compression, if needed. This module is currently configured to run lossy or lossless data compression routines either internal or external to PACEOS™ and to accept data stream formations and downlink effects calculated offline. Effects simulated in this module are removed in the data stream ingest module of the ground processing system. Thus, all functionality exists within the PACEOS™ architecture to perform complete end-to-end simulations and quantitatively assess the value of any system design concept on the retrieved SST_S EDR.

3. Theoretical basis for simulations

The primary goal of these end-to-end computer simulations is to quantitatively evaluate system design concepts on the retrieved accuracy of the SST_S EDR in a laboratory environment to ensure a proposed design will allow system-level requirements to be met once the NPOESS satellites are in orbit. Thus, it is imperative that all aspects of the real world be accurately modeled in the simulations. Since the phenomenology associated with retrieving SST_S from the VIIRS and CMIS sensors is very different, this research is restricted to design concepts for the VIIRS sensor in cloud-free conditions. A notional channel set centered near 3.7, 10.8, and 12.0 μm was assumed in order to use the multichannel sea surface temperature (MCSST) algorithms developed by NOAA for the retrieval of SST_B from AVHRR imagery (McClain et al. 1983; McClain et al. 1985; Walton 1988). Before more fully describing these simulations, additional background information is useful on the theoretical basis of the MCSST algorithms and some basic concepts on satellite radiometer instrument design that were used to define the simulation scenario.

a. Sea surface temperature retrieval algorithms

The accuracy of satellite-derived sea surface temperature observations depends on the ability of radiometers to view the skin temperature of the ocean with little error introduced by the atmosphere. Water vapor attenuation and the presence of clouds, especially clouds that are optically thin or occupy only a small portion of the pixel, are the primary sources of error in the retrieval of sea surface temperatures (Schluessel et al. 1987; Minnett 1986). Subpixel clouds are expected to occur less often in VIIRS imagery compared to AVHRR data. The horizontal spatial resolution requirement for VIIRS regional imagery is 400 m at nadir and 800 m as a worst case, for example, at edge of scan, while the global requirement is 1.0 km at nadir and 2.4 km as a worst case (VIIRS SRD 1997). The horizontal spatial resolution of regional AVHRR imagery is nominally 1.1 km (4 km for global data) at nadir (Kidwell 1995) but grows to about 6 km at edge of scan. Thus, subpixel cloud cover should become a relatively minor issue during the NPOESS era due to the improved spatial resolution of the VIIRS imagery.

In addition, optically thin cirrus clouds may go undetected in existing AVHRR imagery since the spectral signature of water vapor and thin cirrus clouds are similar in these spectral bands (Hutchison et al. 1995). However, vastly improved thin cirrus screening should be possible with the VIIRS by incorporating new spectral data in which the signature of ice clouds is very different from that of water vapor. For example, the 1.38-μm channel has been shown to be highly beneficial for improved detection of thin cirrus over land surfaces (Hutchison and Choe 1996; Gao et al. 1993). This imagery would be even more beneficial for the detection of thin cirrus over cloud-free ocean surfaces, especially in the humid Tropics, since increased concentrations of lower-level water vapor enhances the signature of higher-level cirrus clouds in this band. Thus, errors in SST_S retrievals resulting from the misclassification of optically thin cirrus clouds in daytime imagery are also expected to become relatively insignificant during the NPOESS era.

On the other hand, water vapor absorption can induce significant errors in satellite-based sea surface temperature analyses, even in cloud-free conditions, since it absorbs energy emitted by the ocean and reradiates it at colder temperatures typical of the atmosphere a few kilometers above the surface (Stewart 1985). The MCSST algorithms have been developed to correct satellite observations for atmospheric water vapor attenuation in order to accurately specify SST_B under a wide range of ocean surface temperatures and atmospheric conditions (Walton 1988; Hagan 1989; McClain et al. 1985; McMillin and Crosby 1984; McClain et al. 1983). These algorithms correct the 10.8-μm brightness temperature, which is the AVHRR band that most closely approximates the ocean surface temperature, for water vapor absorption using brightness temperature differences between the 3.7- and 12.0-μm channels in nighttime data and the 10.8- and 12.0-μm bands in the daytime when solar contamination renders the 3.7-μm chan-

nel less valuable (McClain et al. 1985). Since water vapor attenuation is least in the 3.7-μm channel and greatest in the 12.0-μm band (Hutchison et al. 1995), the three-channel MCSST would be expected to more accurately estimate the total water vapor present in the atmosphere and allow a more accurate correction than is possible with the two-channel algorithm. Statistics on the performance of the MCSST algorithms confirm this since nighttime SST_B observations have root-mean-square difference (rmsd) values that are smaller than those found with daytime data (McClain et al. 1985; McClain et al. 1983; Kenley 1994).

Coefficients in the MCSST algorithms have been computed by regression of satellite-retrieved sea surface temperatures (i.e., SST_B) against those measured primarily by drifting buoys (Strong and McClain 1984). Since in situ observations of sea surface temperatures are only sporadically collected by research vessels, similar regression coefficients are not yet available for the retrieval of SST_S from satellite observations; however, studies have been completed to quantify the error introduced by differences between these reference temperatures. In general, these differences tend to be on order of 0.1–0.3 K but can be as large at 1.0 K or more (Wick et al. 1992; Schluessel et al. 1990). This means that differences between skin and bulk reference temperatures can cause discrepancies in the simulations that are nearly as large as the SST_S accuracy requirement.

b. Basic concepts on satellite radiometer instrument design

The sensitivity of radiometers depends on the ratio of their internally generated signal to that produced by incoming radiation (Stewart 1985). The power available to the instrument is given by

$$\Phi_{IN} = Ad\Omega d\lambda L(\lambda), \tag{4}$$

where A is the aperture of the instrument, $d\Omega$ is the angular extent of the area viewed by the instrument, $d\lambda$ is the bandwidth, and $L(\lambda)$ is the spectral radiance of the area viewed. The power is usually focused on a detector that converts radiant power into electrical power, which is then amplified and either recorded or transmitted to the ground. The output of the detector Φ_{OUT} is the sum of the incoming signal Φ_{IN} plus the noise $\Delta\Phi$ generated within the transducer and is represented as

$$\Phi_{OUT} = Ad\Omega d\lambda L(\lambda) + \Delta\Phi. \tag{5}$$

The signal-to-noise ratio S_n of the instrument is then given by

$$S_n = \Phi_{IN}/\Delta\Phi \sim [Ad\Omega d\lambda L(\lambda)]/\Delta\Phi. \tag{6}$$

The optimal sensor design maximizes S_n in a cost-effective manner, which may only be done in a couple ways. First, S_n may be enlarged by increasing the size of the aperture (A), the field of view ($d\Omega$), and/or the bandwidth ($d\lambda$). Second, it is possible to increase S_n by reducing $\Delta\Phi$, which is done with improved detector performance. Often the instrument noise is inserted into the Planck equation and converted to an apparent change in temperature ΔT, which is referred to as the noise equivalent ΔT or NEΔT.

Another option to maximize the function S_n is to observe the area N times with the same instrument, assuming L does not change between observations. The average of these observations converge toward Φ_{IN} as N increases. If the noise in different observations is not correlated, then on average

$$S_n = (N)^{0.5}[Ad\Omega d\lambda L(\lambda)]/\Delta\Phi. \tag{7}$$

c. The simulation approach

Clearly, several options are available to assess sensor performance characteristics in order to provide the satellite observations necessary to retrieve global sea surface temperatures. In general, concept studies seek to maximize S_n, as shown in Eq. (7), while minimizing costs in order to optimize a design. For example, it is possible to take multiple observations of each field of view as is done with the along-track scanning radiometer (ATSR) flown on the ERS satellite series (Za'vody 1995). In addition, the aperture A can also be increased at the expense of making the instrument larger. The field of view can also be increased; however, spatial resolution must be balanced against the increase in $d\Omega$ and horizontal cell size, which relates to field of view, as defined by the NPOESS program. Cooling sensor detectors to lower temperatures can be used to decrease the NEΔT. Finally, channel bandwidth is constrained by atmospheric windows available for exploitation by an imaging sensor and the phenomenology associated with the sea surface temperature retrieval algorithm. As an example, it may be desirable to simultaneously minimize solar contamination and maximize atmospheric transmission in the 3–5-μm window, which together may define a preferred spectral bandpass.

While all these approaches are viable candidates for simulation studies, not all are practical, for example, cooling detectors may be relatively expensive, while employing the ERS scan geometry may negatively impact the retrieval of other EDRs required from the VIIRS sensor. Thus, it was determined that the goal of these simulations would be to examine the impact of the more stringent NPOESS SST_S measurement accuracy requirement on NEΔT for a notional VIIRS sensor with infrared bandpasses closely resembling those of the AVHRR sensor, which enables SST_S to be retrieved using existing MCSST algorithms. Differences between the sea surface temperature references (i.e., SST_B versus SST_S) are accounted for as a bias in the calibration run.

A series of simulated radiances were generated for a sensor in a nominal near-polar, sun-synchronous orbit of 850 km. The sensor viewed a cloud-free, 100 $\times$ 100 pixel array (10 000 in total) in spectral bands centered

near 3.7, 10.8, and 12.0 μm; and, ocean surface emissivity values were assumed to be 0.96, 1.0, and 0.99, respectively. Since NEΔT has its greatest impact on the coldest temperature in the required measurement range, that is, 271–313 K, only the minimum SST_S was used in the simulations, that is, each pixel was assigned an initial value of 271 K. Upwelling radiances were generated with MODTRAN, assuming a nadir scan position and using a midlatitude winter atmospheric profile along with a surface visibility of 23 km (Berk 1989). No additional tropospheric or stratospheric aerosols were included in the simulations.

Once upwelling radiances were computed in the three spectral bands, instrument noise was added randomly to each set of simulations corresponding to NEΔT having a mean of 0.0 and 1σ values of 0.0, 0.05, 0.1, and 0.3 K. This resulted in a total of 120 000 data points for the complete simulation (10 000 pixels $\times$ 3 bands $\times$ 4 NEΔTs). For simplicity, the NEΔT values in each spectral band were assumed to be identical. Furthermore, the response function of each channel in the notional sensor was assumed to be a step function. Energy recorded by the detectors was calibrated, and SST_S values were retrieved from the derived brightness temperatures using the MCSST algorithms (McClain et al. 1983; McClain et al. 1985; Walton 1988). The retrieval of SST_S from daytime imagery employed channels centered at 10.8 and 12.0 μm, while SST_S retrieved from nighttime imagery included these data along with those in the 3.7-μm band. Finally, an error analysis was completed to ensure that 1) ''real-world'' phenomenology was accurately modeled in the simulations, 2) algorithm error was fully quantified, and 3) available error could be allocated to satellite system components.

4. Results

These end-to-end simulations are not intended to be critical of any current retrieval algorithm or methodology nor are the results intended to be exhaustive, definitive, or to demonstrate a new retrieval methodology, algorithm, or sensor design concept. While these are worthy objectives, the focus of our initial simulations is to understand the basic components of algorithm or modeling errors and system hardware errors related to total system error in an end-to-end simulation environment. Thus, the primary purposes of these end-to-end simulations are 1) to evaluate the capability of modeling real-world phenomenology with PACEOS™ scene simulation software and 2) to perform a thorough assessment of all algorithm (modeling) errors as a prerequisite for conducting more meaningful system-level trade studies that may be needed to meet the more stringent SST_S accuracy requirements. As previously noted, the approach was to examine the impact of the more stringent NPOESS SST_S measurement uncertainty requirement on NEΔT for a notional VIIRS sensor with infrared bandpasses closely resembling those of the AVHRR sensor, which enables SST_S to be retrieved using existing MCSST algorithms.

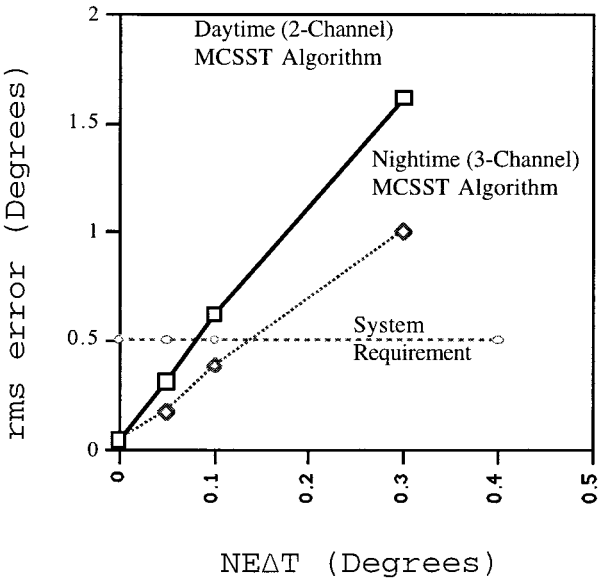

FIG. 2. Measurement uncertainty (1σ) in retrieved sea surface skin temperatures as a function of NEΔT for a notional sensor with bandpasses centered at 3.7, 10.8, and 12.0 μm using NOAA's MCSST daytime and nighttime algorithms.

a. Retrieval of sea surface temperatures from PACEOS™ simulated radiances

An internal check on the simulation procedures was completed by initializing the temperatures of all 10 000 pixels to 271 K and generating upwelling radiances with PACEOS™ while assuming no atmospheric attenuation and setting the sensor NEΔT to zero. The resulting radiances were converted to brightness temperatures and compared with the input sea surface temperature field as a verification of the calibration procedures. The brightness temperatures were then used to retrieve SST_S with the MCSST algorithms and establish a modeling bias so the MCSST algorithms could be utilized to retrieve SST_S. The remaining simulations were completed using a midlatitude winter atmospheric profile with the given values of NEΔT.

Results of the end-to-end simulations are shown in Fig. 2, and upon inspection it appears that a sensor NEΔT value of about 0.08 K is required to meet the NPOESS SST_S EDR threshold requirement if only 10.8- and 12.0-μm data are used in the retrieval, based upon the standard (daytime) two-channel MCSST algorithm. On the other hand, the requirements are satisfied with an NEΔT as large as about 0.12 K if the additional 3.7-μm channel is included in the analysis and the standard three-channel (nighttime) MCSST algorithm is applied. For the present, it is assumed that system costs make the 0.12-K NEΔT a preferred solution.

Therefore, an optimal system design might use three

TABLE 1. Conversion of AVHRR sensor specifications of NEΔT to correspond with sea surface temperatures in the measurement range of 271–313 K (J. Sullivan 1997, personal communication).

Wavelength (μm)	Noise-equivalent delta temperature (K)				
	271	280	290	300	313
3.7	0.383	0.260	0.174	0.12	0.077
10.8	0.159	0.145	0.131	0.12	0.108
12.0	0.153	0.141	0.129	0.12	0.110

channels of infrared imagery during daytime and nighttime conditions in order to satisfy the EDR measurement uncertainty SST_S requirement in the NPOESS era using the current MCSST algorithms. Thus, it appears that one recommendation from these simulations would be to identify an additional VIIRS channel for use with the daytime algorithm. However, an alternative approach might keep the NEΔT at about 0.12 K and employ an enhanced retrieval algorithm that uses only two channels of daytime imagery with information from another NPOESS sensor, for example, total water vapor from the CMIS sensor (Emery et al. 1994). To further examine which option is preferable, more detailed analyses are needed to understand the reason the three-channel nighttime algorithm outperforms the two-channel daytime algorithm.

b. Analysis of modeling errors associated with the MCSST algorithms

Simulations may fail to accurately consider all aspects of real-world phenomenology so it is highly useful to assess algorithm error from the analysis of actual sensor data when possible. Fortunately, the MCSST algorithms have been studied extensively, and results are available in the literature. These data are invaluable for characterizing the modeling errors associated within the retrieval of SST_B values from actual AVHRR satellite data, which has a NEΔT sensor design specification of 0.12 K at 300 K for each of the infrared channels.

From Table 1 of McClain et al. (1983), the rmsd between observed and satellite-retrieved SST_B in daytime imagery is shown to be 0.78 K based upon the two-channel algorithm that uses brightness temperatures of AVHRR spectral data centered at 10.8 and 12.0 μm, that is, $T_{10.8}$ and $T_{12.0}$, respectively, using the estimation equation

$$SST_{10.8/12.0} = 1.035T_{10.8} + 3.046(T_{10.8} - T_{12.0}) - 283.93. \quad (8)$$

Using first-order error analysis, Kenley (1994) found that there is an error due to the uncertainty in the satellite observations and a residual error due to inaccuracies in algorithmic modeling that, for the daytime algorithm, can be expressed as

$$0.78^2 = \text{residual}^2_{10.8/12.0} + (4.081\sigma_{10.8})^2 + (3.046\sigma_{12.0})^2. \quad (9)$$

By inserting the AVHRR sensor specification NEΔT values of 0.12 K for each channel into Eq. (9), the residual or algorithm error can be readily calculated as

$$0.78^2 = \text{residual}^2_{10.8/12.0} + (4.081 \times 0.12)^2 + (3.046 \times 0.12)^2 \quad \text{and} \quad (10)$$

$$\text{residual}_{10.8/12.0} = 0.485 \text{ K}. \quad (11)$$

Thus, the retrieved SST_B error predicted for the two-channel (daytime) MCSST algorithm as a function of sensor NEΔT at sea surface temperatures of 300 K is given by

$$SST_{10.8/12.0} = [(0.485)^2 + (4.081\sigma_{10.8})^2 + (3.046\sigma_{12.0})^2]^{0.5}. \quad (12)$$

Similarly, the rmsd calculated between the observed and satellite-retrieved SST_B values using AVHRR spectral data centered at 3.7, 10.8 and 12.0 μm, that is, $T_{3.7}$, $T_{10.8}$, and $T_{12.0}$, respectively, is calculated to be 0.58 K for the nighttime three-channel algorithm (McClain et al. 1983):

$$SST_{3.7/10.8/12.0} = 1.060T_{10.8} + 1.038(T_{3.7} - T_{12.0}) - 289.55. \quad (13)$$

The residual or modeling error for the three-channel (nighttime) algorithm can be expressed as (Kenley 1994)

$$0.58^2 = \text{residual}^2_{3.7/10.8/12.0} + (1.060\sigma_{10.8})^2 + (1.038\sigma_{3.7})^2 + (1.038\sigma_{12.0})^2 \quad (14)$$

$$\text{residual}_{3.7/10.8/12.0} = 0.538 \text{ K}. \quad (15)$$

Thus, the retrieved SST_B error predicted for the three-channel MCSST algorithm, as a function of sensor NEΔT at sea surface temperatures of 300 K may be calculated using

$$SST_{3.7/10.8/12.0} = [(0.538)^2 + (1.06\sigma_{10.8})^2 + (1.038\sigma_{10.8})^2 + (1.038\sigma_{12.0})^2]^{0.5}. \quad (16)$$

As previously noted, NEΔT varies with temperature; thus, it is useful to also examine the residuals in the MCSST algorithm at the centroid of sea surface temperatures used to develop the regression coefficients. Table 1 shows the conversion of the 300-K AVHRR NEΔT design specification for *NOAA-11* to 280 and 290 K as well as the extremes of the NPOESS SST_S EDR measurement range (J. Sullivan 1997, personal communication).

5. Discussion

Results from the end-to-end simulations suggest that a sensor NEΔT specification of about 0.12 K would allow the NPOESS SST_S measurement uncertainty requirement to be satisfied using the bias-corrected MCSST algorithm approach with three spectral bands of information. However, performance of the MCSST

algorithms with actual AVHRR imagery, which has a NEΔT design specification of 0.12 K, shows this is not the case. Thus, this system-level analysis clearly demonstrates two important results. First, the algorithm or modeling errors associated with the MCSST algorithms consumes most of the error budget for the VIIRS sensor and second, additional phenomenological studies are needed to reduce the residuals in the sea surface temperature retrieval algorithms.

The modeling errors for the two-channel daytime and three-channel nighttime MCSST algorithms at 300 K were calculated to be 0.485 and 0.538, respectively. (If the centroid of the actual SST distribution used to generate the rmsd for the MCSST algorithms was 290 K rather than 300 K, the residuals would be slightly different, that is, 0.410 for the two-channel algorithm and 0.516 for the three-channel algorithm based upon NEΔT values shown in Table 1. These differences do not impact the results or conclusions herein.) Thus, the residuals for the retrieval of SST_B with the MCSST algorithms take up between 97% and 108% of the NPOESS SST_S EDR error budget. Clearly, these large modeling errors are detrimental to meeting the NPOESS measurement uncertainty requirement of 0.5 K and preclude the possibility of satisfying the objective of 0.1 K (VIIRS SRD 1997).

The value of the three-channel MCSST algorithm is that it is less sensitive to sensor NEΔT than the two-channel algorithm. At 300 K, the NEΔT in each channel is 0.12 K and Eq. (9) can be written as

$$SST^2_{10.8/12.0} = \text{residual}^2_{10.8/12.0} + (5.092)^2\sigma^2, \quad (17)$$

and Eq. (14) becomes

$$SST^2_{3.7/10.8/12.0} = \text{residual}^2_{3.7/10.8/12.0} + (1.811)^2\sigma^2. \quad (18)$$

Assuming that residuals can be made comparable due to improved knowledge of SST_s retrieval phenomenology, smaller measurement errors are predicted with a three-channel algorithm due solely to the magnitude of the regression coefficients, that is, 1.811 for the three-channel algorithm shown in Eq. (18) compared to 5.092 for the two-channel algorithm seen in Eq. (17).

A potential weakness of simulations is that they may not accurately model real-world processes. For example, simulation results may be impacted by imperfect radiative transfer modeling. Initial simulations designed to specify sensor characteristics for retrieving ocean surface temperatures from satellites were hampered by inaccuracies in radiative transfer models (Anding and Kauth 1970; McMillin and Crosby 1984). Improvements in modeling radiative transfer processes resulted in a more accurate specification of atmospheric water vapor absorption characteristics that were needed to refine bandpass selections and ultimately led to the split-window infrared channels in the AVHRR sensor (Maul and Sidran 1972; Anding and Kauth 1972).

Similarly, simulation scenarios may also fail, either by design or unintentionally, to account for all significant real-world phenomenological processes. For example, the MCSST algorithms were designed to retrieve SST_B by correcting satellite observations for atmospheric attenuation due to water vapor using a linear regression technique (McClain et al. 1983; Strong and McClain 1984; McClain et al. 1985; Walton 1988). Early results suggested this could be accomplished with an accuracy of 1 K (McMillin and Crosby 1984). As the phenomenology of the retrieving SST_B from satellite observations became better understood, the MCSST algorithms were subsequently updated to compensate for atmospheric attenuation in more moist conditions by using a nonlinear model (Walton 1988). Further attempts to improve the accuracy of SST_B analyses suggest several additional phenomenological processes must be considered, including compensating for surface emissivity variations (Watts et al. 1996; Smith et al. 1996) and possibly ocean wave characteristics (Watts et al. 1996). In addition, other issues previously recognized are yet to be fully modeled, including corrections for atmospheric aerosols (Jacobowitz and Coulson 1973) and reflected sky radiance (Maul 1981; Watts et al. 1996). None of these additional phenomenological effects were modeled in the generation of simulated radiances or addressed in the retrieval of SST_S with the MCSST algorithms; however, the large residuals associated with the retrieval of the sea surface temperatures shown in Eqs. (11) and (15) suggest further improvements are needed in these areas during the NPOESS era.

Considerable effort has been expended on modeling atmospheric processes that are necessary to improve sea surface temperatures retrieval algorithms, and much of this additional work has been summarized in the literature (Barton 1995). Of particular interest is the use of a priori water vapor information to better correct for atmospheric attenuation over split-window techniques. This approach has shown promise both for the retrieval of SST_B and detection of thin cirrus clouds (Emery et al. 1994; Hutchison et al. 1995). While a similar approach has been demonstrated with HIRS data (Wick et al. 1992; Schluessel et al. 1987), microwave imagery provides the most accurate measure of total column water vapor but requires the addition of a moisture profiler to help translate this information into atmospheric layers. An algorithm has been developed that integrates total integrated water vapor into the retrieval of water vapor profiles from microwave sensors (Wilheit et al. 1994); however, these products have yet to be fully evaluated on a global scale in the retrieval of SST_B analyses since both microwave instruments fly only on the DMSP satellites, which do not currently carry a multichannel infrared imaging radiometer. Thus, additional efforts are needed to further improve algorithm modeling through the foreseeable future.

More acceptable in situ observations of SST_S are needed to resolve ambiguities between the end-to-end simulations and SST_B analyses of AVHRR imagery.

These simulations assumed that the retrieval of SST_S and SST_B can be achieved with equal accuracy using the MCSST algorithms, given an ample supply of in situ measurements of sea surface skin temperatures. In reality, SST_S may be retrieved more accurately than SST_B. Infrared satellite measurements only apply to a very thin surface layer of the ocean (Grassl 1976; Paulson and Simpson 1981; Robinson et al. 1984), which is more sensitive to diurnal heating, evaporation, and the presence of near-surface aerosols (Schluessel et al. 1987; Smith et al. 1996) than the shallow mixed surface layer represented by the SST_B. On the other hand, buoy measurements are made at greater depths, which experience more vertical mixing (Wick et al. 1992; Schluessel et al. 1990). Differences between these two references temperatures has been estimated at about 0.1 K during the daytime and 0.3 K during the night but may vary by as much as $\pm 1.0°$ as extremes (Schluessel et al. 1990), which may explain the residual being larger for the nighttime compared to the daytime algorithm. Thus, modeling errors associated with the performance of the MCSST algorithms and other retrieval methods need to be fully quantified against in situ measurements of ocean skin temperatures.

Finally, more comprehensive results on modeling errors are needed for future end-to-end simulations with either the MCSST algorithms or any alternative algorithms. Due to a lack of data in the literature, this analysis assumed that the rmsd between observed and satellite-retrieved SST_B are constant over the sea surface temperatures measurement range 290–300 K for both the daytime and nighttime MCSST algorithms. In all probability, this assumption is not valid; however, adequate information on the SST_B retrieval accuracy was not available. When and if additional in situ data becomes available, the analysis of algorithm error should be completed for many smaller (e.g., 1°–5°) temperature intervals over the entire SST_S measurement range of 271–313 K.

6. Conclusions

Simulations have been performed to better understand the implications of the more stringent NPOESS SST_S measurement uncertainty requirements on the design of a notional VIIRS sensor with characteristics similar to those of the current operational AVHRR sensor. In this case, the simulations assessed the feasibility of satisfying these requirements as a function of sensor $NE\Delta T$ using existing MCSST algorithms that were designed to retrieve SST_B by correcting satellite observations for atmospheric attenuation, which are due primarily to water vapor.

Results from the end-to-end simulations indicate that the NPOESS SST_S measurement uncertainty requirement might best be satisfied using the current MCSST algorithmic approach and three-channels of infrared imagery with design parameters similar to those of the current operational AVHRR sensor. However, residuals in both the two-channel (daytime) and three-channel (nighttime) MCSST algorithms consume the majority of the NPOESS SST_S EDR error budget leaving little or no margin for other spacecraft subsystems. These large modeling errors are detrimental to meeting the NPOESS measurement uncertainty requirement of 0.5 K and preclude the possibility of satisfying the objective of 0.1 K. Thus, a more robust algorithm or a new retrieval methodology may be needed to meet SST_S measurement uncertainty requirements during the NPOESS era. Any new algorithm development should be referenced against in situ observations of ocean surface skin temperature rather than buoy data that have been used to date.

End-to-end simulations serve two important areas of scientific investigation. They support 1) phenomenological studies in which the value of new algorithm methodologies or additional spectral data can be quantitatively evaluated and 2) system concept studies that seek to maximize hardware performance for a particular retrieval algorithm or methodology. To be useful, end-to-end simulations must accurately model real-world phenomenology and employ retrieval algorithms with modeling errors that are thoroughly characterized, which is best accomplished with real sensor data. When these conditions are satisfied, meaningful system-level design trade studies can be completed.

REFERENCES

Anding, D., and R. Kauth, 1970: Estimation of sea surface temperature from space. *Remote Sens. Environ.,* **1,** 217–220.

——, and ——, 1972: Reply to the comment by G. A. Maul and M. Sidran. *Remote Sens. Environ.,* **2,** 171–173.

Barton, I. J., 1995: Satellite-derived sea surface temperatures: Current status. *J. Geophys. Res.,* **100** (C5), 8777–8790.

Berk, A., 1989: MODTRAN: A moderate resolution model for LOWTRAN-7. Tech. Rep. 89-0122, USAF Geophysics Laboratory, Hanscom AFB, 146 pp. [Available from AFGL/DAA, Hanscom AFB, MA 01731.]

Clancy, R. M., and W. D. Sadler, 1992: The Fleet Numerical Oceanography Center of oceanographic models and products. *Wea. Forecasting,* **7,** 307–327.

Clough, S. A., F. X. Kneizys, E. P. Shettle, and G. P. Anderson, 1986: Atmospheric radiance and transmittance: FASCOD2. *Proc. Sixth Conf. on Atmospheric Radiation,* Williamsburg, VA, Amer. Meteor. Soc., 141–144.

Emery, W. J., Y. Yu, G. A. Wick, P. Schluessel, and R. W. Reynolds, 1994: Correcting infrared satellite estimates of sea surface temperature for atmospheric water vapor attenuation. *J. Geophys. Res.,* **99** (C3), 5219–5236.

Falcone, V. J., L. W. Abreu, and E. P. Shettle, 1979: Atmospheric attenuation of millimeter and submillimeter waves: Models and computer code. Tech. Rep. 79-0253, USAF Geophysics Laboratory, Hanscom AFB. [Available from AFGL/DAA, Hanscom, AFB, MA 01731.]

Gao, B. C., A. F. H. Goetz, and W. J. Wiscombe, 1993: Cirrus cloud detection from airborne imaging spectrometer data using the 1.38-micron water vapor band. *Geophys. Res. Lett.,* **20,** 301–304.

Grassl, H., 1976: The dependence of the measured cool skin of the ocean on wind stress and total heat flux. *Bound.-Layer Meteor.,* **10,** 465–474.

Hagan, D. E., 1989: A basic limitation of the split window method for SST retrievals when applied to a wide range of water vapor conditions. *Geophys. Res. Lett.*, **16,** 815–817.

Houghton, J. T., G. J. Jenkins, and J. J. Ephraums, 1990: *Climate Change—The IPCC Scientific Assessment.* University of Cambridge, 364 pp.

Hutchison, K. D., and N. Choe, 1996: Application of 1.38-μm imagery for thin cirrus detection in daytime imagery collected over land surfaces. *Int. J. Remote Sens.,* **17,** 3325–3342.

——, K. R. Hardy, and B. C. Gao, 1995: Improved detection of optically thin cirrus clouds in nighttime multispectral meteorological satellite imagery using total integrated water vapor information. *J. Appl. Meteor.,* **34,** 1161–1168.

Jacobowitz, H., and K. L. Coulson, 1973: Effects of aerosols on the determination of the temperature of the Earth's surface from radiance measurements at 11.2 μm. NOAA Tech. Rep. NESS 66, 18 pp.

Kenley, C. R., 1994: Preliminary surface temperature requirements analysis, Engineering Memo. 1147, Lockheed Missiles and Space Company, 10 pp. [Available from the NPOESS Technical Library]

Kidwell, K. B., 1995: *NOAA Polar Orbiter Data Users' Guide.* NOAA NESDIS, 257 pp.

Marusa, S., R. A. Rivera, K. D., Hutchison, and W. Uplinger, 1997: Use of MODTRAN Software in performance and analysis capability for earth observation systems (PACEOS™) Software, *Proc. 20th Conf. on Atmospheric Radiance and Transmission Modeling,* Hanscom AFB, MA.

Maul, G. A., 1981: Application of GOES visible–infrared data to quantifying mesoscale ocean surface temperatures. *J. Geophys. Res.*, **86** (C9), 8007–8021.

——, and M. Sidran, 1973: Atmospheric effects on ocean surface temperature sensing from the NOAA satellite scanning radiometer. *J. Geophys. Res.*, **78** (12), 1909–1916.

McClain, E. P., W. G. Pichel, C. C. Walton, A. Ahmad, and J. Sutton, 1983: Multichannel improvements to satellite-derived global sea surface temperatures. *Adv. Space Res.,* **2** (6), 43–47.

——, ——, and ——, 1985: Comparative performance of AVHRR-based multichannel sea surface temperatures. *J. Geophys. Res.,* **90** (C6), 11 587–11 601.

McMillin, L. M., and D. S. Crosby, 1984: Theory and validation of the multiple window sea surface temperature technique. *J. Geophys. Res.,* **89** (C3), 3655–3661.

Minnett, P. J., 1986: A numerical study of the effects of anomalous North Atlantic atmospheric conditions on the infrared measurement of sea surface temperature from space. *J. Geophys. Res.,* **91** (C7), 8509–8521.

Paulson, C. A., and J. J. Simpson, 1981: The temperature difference across the cool skin of the ocean. *J. Geophys. Res.,* **86,** 11 044–11 054.

Robinson, I. S., N. C. Wells, and H. Charnock, 1984: The sea surface thermal boundary layer and its relevance to the measurement of sea surface temperature by airborne and spaceborne radiometers. *Int. J. Remote Sens.,* **5,** 19–45.

Schluessel, P., H.-Y. Shin, and W. J. Emery, 1987: Comparison of satellite-derived sea surface temperatures with in situ skin measurements. *J. Geophys. Res.,* **92** (C3), 2859–2874.

——, W. J. Emery, H. Grassl, and T. Mammen, 1990: On the bulk–skin temperature difference and its impact on satellite remote sensing of sea surface temperature. *J. Geophys. Res.,* **95** (C8), 13 341–13 356.

Smith, W. L., and Coauthors, 1996: Observations of the infrared radiative properties of the ocean—Implications for the measurement of sea surface temperature via satellite remote sensing. *Bull. Amer. Meteor. Soc.,* **77,** 41–51.

Stewart, R. H., 1985: *Methods of Satellite Oceanography.* University of California Press, 360 pp.

Strong, A. E., and E. P. McClain, 1984: Improved ocean surface temperatures from space—Comparisons with drifting buoys. *Bull. Amer. Meteor. Soc.,* **65,** 138–142.

VIIRS SRD, 1997: Visible Infrared Imager Radiometer Suite (VIIRS) sensor requirements document (SRD), for the National Polar-Orbiting Operational Environmental Satellite System Spacecraft and Sensors, Associate Directorate for Acquisition, NPOESS Integrated Program Office, Silver Spring, MD.

Walton, C. C., 1988: Nonlinear multichannel algorithm for estimating sea surface temperature with AVHRR satellite data. *J. Appl. Meteor.,* **27,** 115–124.

Watts, P. D., M. R. Allen, and T. J. Nightingale, 1996: Wind speed effects on sea surface emission and reflection for the Along-Track Scanning Radiometer. *J. Atmos. Oceanic Technol.,* **13,** 126–141.

Webster, F., and M. Fieux, 1984: TOGA Overview. *Large-Scale Oceanographic experiments and Satellites,* C. Gautier and M. Fieux, Eds., D. Reidel, 17–24.

Wick, G. A., W. J. Emery and P. Schluessel, 1992: A comprehensive comparison between satellite-measured skin and multichannel sea surface temperature. *J. Geophys. Res.*, **97** (C4), 5569–5595.

Wilheit, T. T., K. D. Hutchison, and K. R. Hardy, 1994: A water vapor profiling algorithm for advanced environmental monitoring satellites. *Proc. Seventh Conf. on Satellite Meteorology and Oceanography,* Monterey, CA, Amer. Meteor. Soc., 528–531.

Za'vody, A. M., C. T. Mutlow, and D. T. Llewellyn-Jones, 1995: A radiative transfer model for sea surface temperature retrieval for the along-track scanning radiometer. *J. Geophys Res.,* **100** (C1), 937–952.